Uncertainty analysis of the estimation of a rainfall threshold estimate for stony debris flow rainfall threshold: based on the application to the Backward Dynamical Approach

Marta Martinengo[1], Daniel Zugliani[1], and Giorgio Rosatti[1]

[1]Department of Civil, Environmental and Mechanical Engineering, University of Trento, Trento, Italy

Abstract. Rainfall thresholds, namely rainfall intensity-duration A rainfall threshold is a function of some characteristic rainfall quantities that provides the conditions beyond which the probability of debris flow debris-flow occurrence is considered significant, can be used as a forecasting tool in debris-flow early warning system. Many uncertainties may affect the thresholds calibration and, in turn, the reliability and effectiveness of this tool. The purpose of this study is consequently, its robustness. This study aims to assess the uncertainty in the determination of the estimate of a rainfall threshold for stony debris flow based on the Back Dynamical Approach(BDA) (Rosatti et al., 2019), an innovative method to estimate compute the rainfall duration and averaged intensity strictly related to a measured debris flow. The uncertainty analysis has been computed is computed by performing two Monte Carlo cascade simulations: (i) to assess the variability in the estimate of rainfall conditions event characteristics estimate due to the uncertainty of some of the BDA parameters and in the Back Dynamical Approach parameters and data and (ii) to quantify the impact of this variability on the threshold parameters, obtained by using the frequentist method. Then, the deviation between these analysis outcomes and the values obtained in Rosatti et al. (2019) has been examined. The results highlight calibration. This procedure applied to a case study highlights that the variability in the rainfall condition estimate is strongly related to the debris flow characteristics and the hyetograph shape. Depending on these features, the spreading of the obtained distributions can take event characteristics can be both low and highvalues. Instead, the threshold parameters are characterised by a low statistical spreading. Finally, the consistency between the outcome of this study and the results obtained in Rosatti et al. (2019) has been proved and the critical issues related to coefficients have a low dispersion showing good robustness of the threshold estimate. Moreover, the results suggest that some event features are correlated with the variability of the rainfall condition estimation have been discussedrainfall event duration and intensity. The proposed method to assess the uncertainty is suitable to be also applied to other threshold calibration approach.

1 Introduction

Debris flows are very intense phenomena that affect mountain regionsand In mountain regions, rainfall-induced natural phenomena, as shallow landslides and debris flows, are relatively frequent events that have a significant impact on the territory in which they occur, causing damages and, in some cases, casualties (Fuchs et al. (2013), Cánovas et al. (2016)). For this reason, debris flow risk management , based on both active and passive mitigation strategies, (Fuchs et al., 2013; Dowling and Santi, 2014; Cánovas et al., 2016). The risk management of these phenomena is crucial to reduce the effects of the phenomenon their effects on the territory and it is based on both active and passive mitigation strategies. An early warning system is an example of a passive mitigation tool (Huebl and Fiebiger, 2005)

as it allows to activate prevention measures (e.g. evacuation sets out in the civil protection plans) before the expected event occurs. In this last framework, the forecast of the possible occurrence of debris flow is

The early warning systems for these phenomena are mainly based on rainfall thresholds (Chien-Yuan et al. (2005), Segoni et al. (2018)), (Chien-Yuan et al., 2005; Segoni et al., 2018), namely rainfall conditions beyond which the probability of debris flow occurrence occurrence probability of a rainfall-induced event is considered significant. Usually, In this framework, most rainfall thresholds are power laws that link the rainfall duration to the rainfall law relations expressing the rainfall event cumulated or intensity (Nikolopoulos et al., 2014) and the relevant coefficients are calibrated on historical dataas a function of the event duration (Segoni et al., 2018). A considerable literature deals with this topic (e.g. Aleotti (2004), Guzzetti et al. (2007), Jakob et al. (2012), Caine (1980), Guzzetti et al. (2008) , Winter et al. (2010), Jakob et al. (2012), Staley et al. (2013), Marra et al. (2014), Zhou and Tang (2014), Iadanza et al. (2016), Marra et al. (2016) , Pan et al. (2018)).

In some studies rainfall thresholds concern a wide typology of phenomena (Segoni et al., 2018), other works focus on both shallow landslides and debris flows (e.g. Baum and Godt, 2010; Cepeda et al., 2010), other on shallow landslides (e.g. Giannecchini, 2005; Frattini et al., 2009) and finally some studies are specifically conceived for debris flow (e.g. Nikolopoulos et al., 2014; Giannecchini et al., 2016; Li et al., 2016).

Power-law thresholds can be derived in the following way. Given a historical dataset of rainfall-induced events, the rainfall associated with each event is determined and described in terms of the couple of synthetic quantities employed in the threshold (e.g. rainfall event cumulated - event duration). Classically, these quantities are defined only on the basis of a hyetograph analysis (Segoni et al., 2018), without considering the characteristics of the rainfall-induced phenomenon. In a log-log plane, the resulting set of couples becomes a cloud of points and the power-law function is a straight line. Starting from these couples set, the threshold is determined by locating the straight line in the log-log plane using one of the several estimate strategies available in the literature, e.g. manual methods, statistical approaches, probabilistic procedures (Guzzetti et al., 2007; Segoni et al., 2018). The result is the calibrated rainfall threshold.

One of the critical issues of the rainfall threshold calibration is the uncertainty related to both data and models parameters (Gariano et al., 2020a)(Gariano et al., 2020b). Here with the term "model", we indicate generically a single equation or a set of operations that, given some input data and model parameters, provide an output. The In the case of the rainfall threshold, the uncertainties derive mainly from direct data error measurements (e.g. in rainfall)and from the estimation of the parameters related to the chosen models used to prepare the data and , from the non-unique definition of the models parameters (e.g. distance within which to select the rain gauge to define the event precipitation) and from the strategy used to calibrate the threshold. The result is an uncertainty framework that can significantly impact the threshold estimation resulting in a not reliable forecasting tool. In this context, uncertainty analysis is required. In general, this type of analysis allows to assess and control the output variability of a given model due to input uncertainties (Helton et al. (2006), Marino et al. (2008) , Pisoni et al. (2018)) and to describe the degree of goodness of the results (Coleman and Steele, 2018). In the present case, the model is the threshold estimation and the relevant uncertainty outcomes provide useful information concerning the reliability and robustness of the threshold. estimate.

This work aims to assess the uncertainty related to the debris-flow threshold estimation based on the Backward Dynamical Approach (BDA), introduced by Rosatti et al. (2019). Given a rainfall event related to a debris flow occurrence, Some studies have already investigated the uncertainty in threshold determination, focusing on some aspects that can affect the hyetograph or the event synthetic quantities used in the threshold. For

instance, Nikolopoulos et al. (2014) has analysed the consequence of the BDA allows to quantify the rainfall volume strictly pertaining to the surveyed debris flow. The rainfall volume is defined as the amount of water needed to convey downstream as a mixture, spatial variability of the precipitation while Marra (2019) and Gariano et al. (2020b) have investigated the effect of the rainfall temporal resolution. Moreover, the uncertainty arising from the choice of the reference rain gauge and the differences between the radar and the rain gauge measurements have been examined in Rossi et al. (2017). Besides, the effect of the uncertainty in triggering rainfall estimate has been investigated in Peres et al. (2018) while Abraham et al. (2020) has analysed the consequences of the scale of analysis, the rain gauge selection and how the intensity is quantified.

Rosatti et al. (2019) has introduced an innovative method to calibrate an intensity-duration rainfall threshold for stony debris flow, a particular type of debris flow, frequent in some mountain areas as in the Alps, in which the presence of silt and/or clay in the mixture is negligible and the internal stresses are mainly caused by the collision among the particles (e.g. Takahashi, 2009; Stancanelli et al., 2015; Bernard et al., 2019). The new method, called Backward Dynamical Approach (BDA), starts from the knowledge of the volume of sediments deposited by the debris flow. It is estimated on the basis of after an event and, thanks to a schematic description of debris flows dynamics. Once the rainfall volume is calculated, the relevant rainfall conditions (duration D and averaged intensity I) determining that volumeis defined based on the event hyetograph. Finally, the threshold calibration is performed applying the frequentist method (Brunetti et al. (2010) and Peruccacci et al. (2012)) to the (I, D) set, obtained considering all the known and well documented events in a homogeneous area.

In literature, there are some studies related, for example, to the variability of calibrated threshold due to the uncertainty in rainfall estimation (estony debris-flow dynamic, it is able to identify, in the related hyetograph, the rainfall event volume, intensity and duration, strictly pertaining to the debris-flow event. g. Nikolopoulos et al. (2014), Rossi et al. (2017)) and in rainfall temporal resolution (Marra, 2019). On the contrary, this Hence, the BDA differs from the classical literature approaches since the synthetic quantities describing the rainfall events are defined involving not only the forcing (i.e. the hyetograph) but also the dynamic of the rainfall-induced event.

This work focuses on the analysis of how the uncertainty in some input parameters affects the BDAoutputs and threshold estimation and not on the rainfall.

The uncertainty analysis can be performed using uncertainty deriving from data and parameters inherent to the BDA, leaving out the uncertainty related to the hyetograph, already investigated in the literature. In particular, the aim is to perform an uncertainty analysis on the threshold calibration to check the robustness of the BDA. To reach the goal, among the different strategies and methods (e.g. Helton et al. (2006), Coleman and Steele (2018), Hofer (2018)). In this paper, available in the literature (e.g. Helton et al., 2006; Coleman and Steele, 2018; Hofer, 2018), we have chosen the Monte Carlo (MC) approach. It consists in the production of a large set of model outputs, obtained picking the model inputs within given ranges. Then, the statistical analysis of the output set gives the required uncertainty estimation. In this work, With this tool, we have developed a proper methodology composed of two MC cascade simulations have and we have applied it to a dataset concerning a specific study area. Detailed analysis of intermediate and final results have also been performed to carry out better understand the uncertainty analysis . A first MC application is used to assess the uncertainty in the BDA outputs estimation. Then, the effects of these outputs variability on threshold calibration are quantified with a further MC computation. Finally, the results are compared with the reference values obtained in Rosatti et al. (2019) to assess their consistency. outcomes.

The paper structure is the following. A brief description of the BDA method and the calibrated threshold obtained by Rosatti et al. (2019) for a study area is presented in Sect. 2. The study area and data are described in Sect. 3. The method used to assess the uncertainty

propagation in the BDA-based threshold calibration is described in Sect. 4. The results of the application of the method obtained are presented
95 obtained results are presented and discussed in Sect. 4. In Sect. 5, discussion and conclusion 5. Conclusions end the paper.

2 The Backward Dynamical ApproachBDA-based threshold calibration

The Backward Dynamical Approach is an innovative method proposed by Rosatti et al. (2019) that defines the rainfall volume strictly relevant As mentioned in the Introduction, the BDA determines the rainfall event intensity and duration, namely the couple (I, D), associated to a stony debris flow in a physical-based way. As described in Rosatti et al. (2019), the BDA starts by using not only the hyetograph but also information
100 concerning the occurred debris flow.

Starting from the knowledge of the deposited volume V_{dep} occupied by the sediments , surveyed after a debris flow event . Thanks after a debris-flow event and thanks to a simplified global volumetric description of the phenomenon debris-flow dynamic (Fig.1), the rainfall volume pertaining to the debris flow V_r^{DF}, defined as the volume of water necessary to convey downstream V_{dep} as a mixturethe volume of sediments V_{dep}, can be express asa function of this latter volume:

$$V_r^{DF} = \frac{c_b - c}{c} V_{dep} \tag{1}$$

where c_b is the concentration of the sediment in the bed, constant and assumed equal to 0.65 (Takahashi, 2014), and c is a reference volumetric solid concentration of the given debris flow. According to Takahashi (1978), c can be estimated as

The expression of Takahashi (1978), valid in permanent and uniform conditions, can be used as reference concentration:

$$c = \min\left(\frac{i_f}{\Delta\left(\tan\psi - i_f\right)}, 0.9\, c_b\right) \tag{2}$$

where i_f is the average slope of the last 50 m of the river bed before the deposition zonei_f is the bed slope, ψ is the dynamic friction angle of the sediments and $\Delta = (\rho^s - \rho^l)/\rho^l$ is the sediment relative submerged density, constant and assumed equal to 1.65 (e.g. Prancevic and Lamb, 2015), where ρ^l and ρ^s are, respectively, the liquid and solid constant density. V_r^{DF} According to the assumptions of the BDA, the reference concentration is evaluated considering the bed slope in the last portion
115 of the debris-flow channel, just upstream of the deposition area. This means that information concerning the triggering conditions and the detailed evolution of the debris flow in the upper part of the basin are not considered.

The rainfall volume pertaining to the debris flow can also be express as product between expressed as the product of the rainfall volume per unit area E and the event basin area A_b:

$$V_r^{DF} = E A_b \tag{3}$$

120 from which, a backward dynamical expression for the rainfall volume per unit area can be obtained by equating (1) with (3):

$$E = \frac{1}{A_b} \frac{c_b - c}{c} V_{dep} \tag{4}$$

Conceptual Lagrangian volumetric description of debris flow dynamic from Rosatti et al. (2019). The scheme is divided into three transepts: transept 1 is characterised by the runoff formation; the bed material erosion and the achievement of equilibrium conditions occur in transept 2; transept 3 is characterised by the deposition of sediments with water

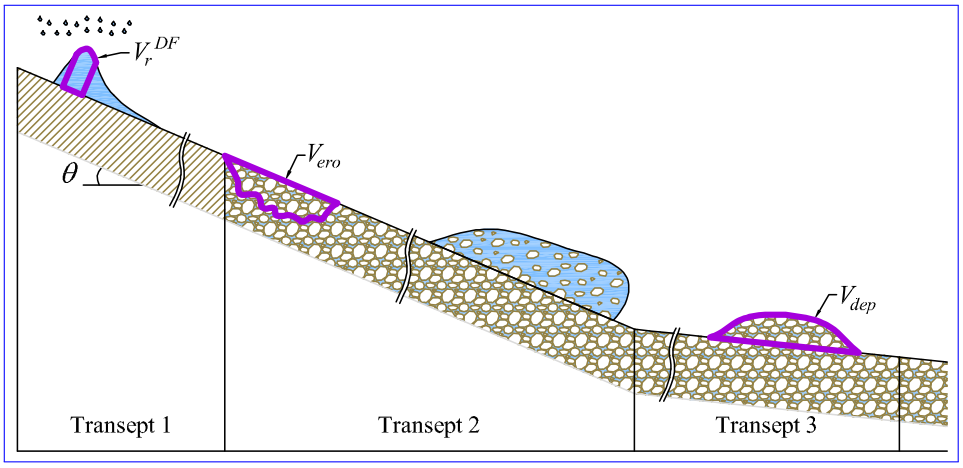

Figure 1. Conceptual Lagrangian volumetric description of debris-flow dynamic from Rosatti et al. (2019). The scheme is divided into three transepts: transept 1 is characterised by the runoff formation; the bed material erosion and the achievement of equilibrium conditions occur in transept 2; transept 3 is characterised by the deposition of sediments with water entrapment. V_r^{DF} is the rain volume pertaining to the debris flow, V_{ero} is the bed volume variation related to the erosion, V_{dep} is the deposited volume occupied by the sediments and $\theta = \arctan(i_f)$ is the inclination angle of the bed with respect to a reference horizontal direction.

entrapment. V_r^{DF} is the rain volume pertaining to the debris flow, V_{ero} is the bed volume variation related to the erosion, V_{dep} is the deposited volume occupied by the sediments and θ is the inclination angle of the bed with respect to a reference horizontal direction.

On the other hand, E can be obtained from the forcing of the phenomenon, namely in the hyetograph. Under the assumption of uniform rainfall over the basin, the hydrological expression for E is:

$$E = \int_{t_1}^{t_2} i(t)\, dt \tag{5}$$

where $i(t)$ is the measured rainfall intensity , and t_1 and t_2 are the unknown start and end times related to the debris-flow duration. In the absence of event detailed data, these times are expressed as:

$$\begin{cases} t_1 = t_{max} - \Delta t_1 \\ t_2 = t_{max} + \Delta t_2 \end{cases} \tag{6}$$

where t_{max} is the instant of maximum intensity during the event t_{max} is assumed to be the debris flow triggering time (Iadanza et al., 2016) and t_1 and t_2 are assumed to be : and Δt_1 and Δt_2 are unknown intervals. These intervals can be obtained equating the right hand side terms of Eq. (5) and (4):

$$\int_{t_{max}-\Delta t_1}^{t_{max}+\Delta t_2} i(t)\, dt = \frac{1}{A_b} \frac{c_b - c}{c} V_{dep} \tag{7}$$

Because of the measurement technique, $i(t)$ is a piecewise constant function on time intervals δt. Therefore, the δt, namely $i(k)$. Consequently, reference times becomes: $t = k\delta t$, $t_{max} = M\delta t$, $\Delta t_1 = n_1\delta t$ and $\Delta t_2 = n_2\delta t$ where M is the number of time intervals that identifies the peak and now n_1 and n_2 are unknown integers. Another consequence is that the integral in Eq. cannot equal exactlythe value of E, and an approximated value must be considered. The values of $\Delta t_1 = n_1\delta t$ and $\Delta t_2 = n_2\delta t$ are computed considering the minimum number of intervals (i.e. n_1 and n_2) necessary to exceed (or equal) the value of E: (7) must be rewritten in discrete form (namely a summation) and that the previous equation cannot be satisfied exactly.

An approximated algorithm, able to determine in an univocal way the unknowns, can be introduced: starting from zero and increasing of one unit alternatively n_1 and n_2, the first couple $\hat{n}_1, \hat{n}_2$ such that

$$\min \int_{t_1}^{t_2} \sum_{k=M-\hat{n}_1}^{M+\hat{n}_2} i(tk)\, dt\delta t \geq E \frac{1}{A_b} \frac{c_b - c}{c} V_{dep} \tag{8}$$

For further details on the computation of Δt_1 and Δt_2, please refer to Rosatti et al. (2019). Thereforeis the searched couple. If a zero-intensity interval is reached, the sum stops being symmetrical with respect to M and only either n_1 or n_2 is increased until the previous relation is satisfied.

Finally, the duration D and the average intensity Irelated to the event become , can be expressed as:

$$D = \Delta t_1 + \Delta t_2 = (\hat{n}_1 + \hat{n}_2)\, \delta t \tag{9}$$

$$I = \frac{\sum_{k=M-\hat{n}_1}^{M+\hat{n}_2} i(k)\, \delta t}{D} \tag{10}$$

2.1 The BDA-based threshold for a study area

As described in Rosatti et al. (2019), the BDA methodology has been applied to obtain a stony debris flow rainfall threshold for Once the (I, D) couple is computed for each event of the Trentino-Alto Adige/Südtirol region (Italy) (Fig. 2). A dataset composed of 84 debris flow events has been considered to calibrate the threshold. Firstly, the (I, D) couples have been computed applying the BDA method. Then, the threshold has been obtained available dataset, the rainfall threshold is estimated by using the frequentist method (e. g. Brunetti et al. (2010) and Peruccacci et al. (2012)). (e.g. Brunetti et al., 2010; Peruccacci et al., 2012) . According to this method, the threshold is a straight line in the (I, D) couples are plotted in a log-log ID plane parallel to the power law and a straight line fitting these points is determined. The slope and the intercept of this straight line are the logarithms of the coefficient of the following power law:

$$I = \hat{a} D^{-b} \tag{11}$$

obtained fitting the events rainfall conditions. The threshold exponent is therefore equal to b while the intercept is computed by setting a value of the The rainfall threshold is then obtained translating vertically the straight line in the log-log ID plane so that the non-exceedance probability of the dataset events , namely by imposing (namely the occurrence probability of debris flows related to rainfall conditions (I, D) points located below the threshold. The threshold equation isthen:) is equal to a given value. The final expression is:

$$I = a D^{-b} \tag{12}$$

in which $a < \hat{a}$.

For more details on the BDA and the frequentist method, we refer the reader to the above-mentioned references. In Rosatti et al. (2019) the non-exceedance level has been set equal to 5% and the resulting calibrated threshold is:

$$I = 6.2D^{-0.67}$$

Location of Trentino-Alto Adige/Südtirol region (Italy), the study area used in Rosatti et al. (2019).

3 Method Study area and data

As briefly presented in The study area and data used in this analysis are the same as those used in Rosatti et al. (2019). In particular, the introduction, to perform a comprehensive study, the uncertainty analysis of the BDA-base threshold estimation is divided into three parts. A first analysis examines the uncertainty propagation in the computation of the BDA outputs (i. e. (I, D) couple, Eq. (9)and (10), study area is the Trentino-Alto Adige/Südtirol region, in the north east of the Italian Alps (Fig. 2(a)). The region covers 13607 km^2, has an altitude range between 40 and 3900 m a.s.l. with mean about 1600 m a.s.l. (Fig. 2(b)) and a climate characterised mostly by a continental regime (Bisci et al., 2004; Nikolopoulos et al., 2014).

The regional agencies between 2006 and related values of c, Eq.(2)2016 have reported 161 debris flows (Fig. 2(b)) but only 139 events present the survey of the deposits, whose volumes range between 100 m^3 and E, Eq. (4)) starting from the uncertainty of some input parameters. Subsequently, 50000 m^3. In every event, sediment are characterised by the absence or, at least, the negligible presence of silt and clay thus resulting as stony debris flows.

The rainfall data associated to these events derives from a radar located in a central position with respect to the region, on the Mt. Macaion at 1866 m a.s.l. (Fig. 2(b)). A C-band Doppler weather radar measures the reflectivity Z over an area of 120 km of radius and the rainfall is computed converting Z into precipitation intensity I (e.g. Uijlenhoet, 2001). Since radar data in mountain regions are typically affected by the beam shielding (Germann et al., 2006) that can cause errors in the measurements, the effects of this propagation on the frequentist method threshold estimation are analysed. Finally, acomparison between the results of the two previous analyses and the reference outcomes, obtained in Rosatti et al. (2019), is carried out. In the following sections, we present the details of each part.

3.1 BDA outputs uncertainty analysis

The main sources of uncertainties in the BDA outputs are attributed to some of the input parameters and data, namely the average slope debris-flow events located in an area with a weakening of the signal greater than 90% are excluded from the dataset. Overall, the debris flows suitable for the analysis were 84 and are highlighted in Fig. 2(b) with circles.

Additional data required for the BDA, namely i_f, the basin area A_b, the deposited volume V_{dep} and the dynamical friction angle ψ . As described in Rosatti et al. (2019), during the calibration phase, i_f and A_b related to each event have been estimated performing GIS analysis based on the available debris flow data (e. g. location of the deposited area , technical reports...) and V_{dep} have been provided by regional agencies. Instead and $i(t)$, was defined for each event in the following way. The basin outlet has been located downstream of a segment with a sufficiently constant slope just upstream of the

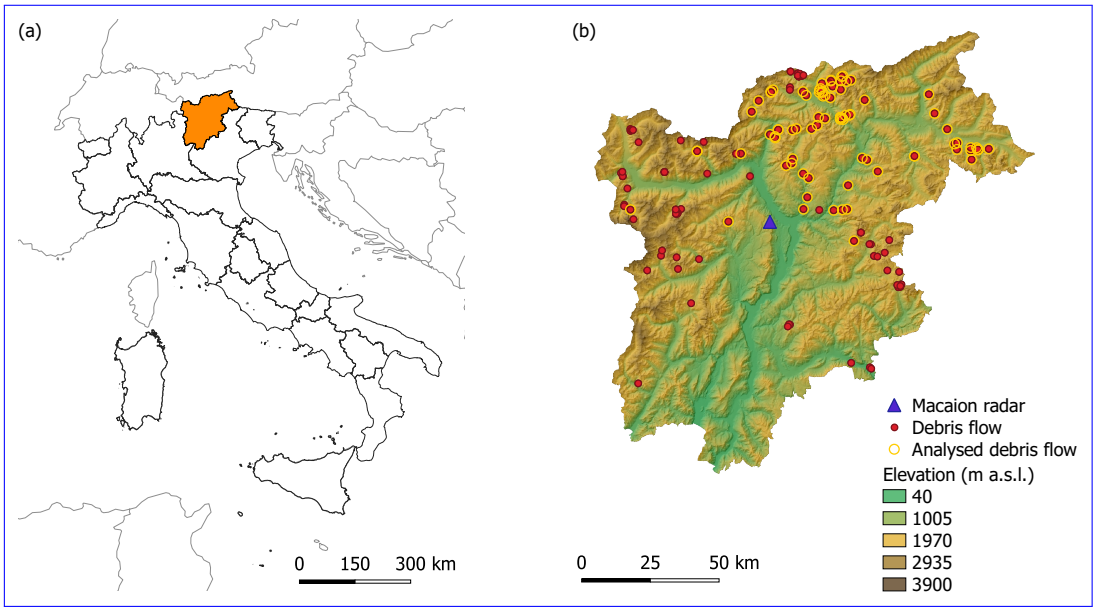

Figure 2. (a) Location of Trentino-Alto Adige/Südtirol region (Italy) and (b) the Macaion radar and debris-flow events: red dots show all debris flows while yellow circles highlight the suitable ones for the study.

deposition area and the upstream basin area was determined. Then, i_f has been calculated as the mean slope of the last 50 m of the torrent upstream of the outlet point. Besides, due to the scarcity of sediments information, ψ has been was assumed to be equal to $35°$ for all debris flow events. As stressed in the Introduction, the rainfall intensities the events. The hyetograph $i(t)$ associated with the event are assumed to be certain. Future analysis will assess and study also the uncertainties related to this piece of data. was computed at each instant averaging over the respective basin area the radar intensities. In this way, both the spatial and temporal variability of the rainfall is taken into account.

For each event, the uncertainty propagation of

Starting from this data and setting the non-exceedance probability equal to 5%, Rosatti et al. (2019) obtained the following threshold:

$$I = 6.2D^{-0.67} \tag{13}$$

From now on, the quantities involved in the calibration performed by Rosatti et al. (2019) will be considered as reference values and they will be indicated with a subscript r.

4 Method

As described in Sect. 2, the BDA-based threshold calibration starts from the definition of the following input parameters and data for each considered event: i_f, A_b, $V_{dep}$and , ψ is carried out with MC approach using the Latin Hypercube Sampling (LHS)procedure

(McKay et al. (2000), Helton and Davis (2003) and Helton et al. (2006))for the generation of the sample. The implementation of this procedure is schematized in and $i(t)$. Subsequently, based on these values, what we call the "event characteristics" are computed for each analysed debris flow: first c (Eq. (2)) and E (Eq. (4)), and then D (Eq. (9)) and I (Eq. (10)). Finally, the (I, D) couples of the events are used to calibrate the threshold, namely to quantify the threshold coefficients a and b of Eq. (12).

Coherently to the estimate procedure, the uncertainty analysis of the BDA-based threshold calibration is divided into three parts (Fig. 3). First, the uncertainty characterisation of the input parameters and data is determined (Fig. 3(a)). Then, for each debris flow, the uncertainty analysis of the event characteristics is performed with an MC simulation, starting from the uncertain quantities above defined (Fig. 3(b)). Finally, a further MC simulation is carried out to perform the uncertainty analysis of the threshold, using as input the (I, D) couples of the events obtained from the first MC simulation (Fig. 3and is composed of three main steps(c)). In this way, the impact of the uncertain parameters and data on the threshold is quantified.

All the analyses are performed using the R software (R Core Team, 2013) and, in the following sections, we present the details of each part. First, the

4.1 Uncertainty characterisation

As explained in the Introduction, in this study, the focus is on the uncertainty in the physical and morphological parameters and data used in the BDA to describe in a simplified way the debris-flow dynamic. Therefore, in this analysis, the variables considered are i_f, A_b, V_{dep} and ψ. According to their estimate described in Sect. 3, these variables are mainly affected by epistemic uncertainty due to measurement and estimate errors and lack of information (Oberkampf et al., 2004).

The characterization of the uncertainty in the parametersvariable, namely the probability distribution function (pdf) of their values, has to be defined (both in term of distribution type and statistical quantities (e.g. mean and variation coefficient CV) (Fig. 3(a)). Lacking certain data concerning the pdfs, according to Marino et al. (2008), all the input parameters variable are assumed to be uniformly distributed . In particularand, for each event, the means of the parameter distributions are set equal to the reference values, namely to the values used in the calibration phase (indicated with subscript r). The dynamical friction angle corresponding reference values.

Regarding the deviations from the means, ψ is the only parameter with variable whose variability is constrained by a validity range. For : for stony debris flow, according to Lane (1953) and Blijenberg (1995), it varies from ψ can vary between $32°$ to and $38°$. Therefore, assuming Assuming $35°$ as the mean of the ψ distribution, this range the variability range $(32°, 38°)$ can be obtained by imposing a variation coefficient CV (i. e. the ratio between the standard deviation and the mean) equal equals to about 5%.

The uncertainty in V_{dep} can not be accurately estimated since the survey methodology, and the related measurement errors, used by regional agencies, is not univocal (Marchi et al., 2019). However, Brardinoni et al. (2012) has proposed for a similar study area a relative error of 10% in the estimate of V_{dep}, namely a corresponding CV equals to about 5%. Since being greater than zero is the only constraint of the other parameters, for homogeneity this CV value is considered suitable for all parameters. The uncertainties characterization of the parameters Therefore, we assume this uncertainty value is valid for this analysis.

Finally, the uncertainty in i_f and A_b is hardly quantifiable given their computation method. For these reasons and homogeneity, the degree of uncertainty of ψ and V_{dep} is considered suitable also for i_f and A_b.

The resulting uncertainty characterization is summarized in Table 1. Second, the parameter

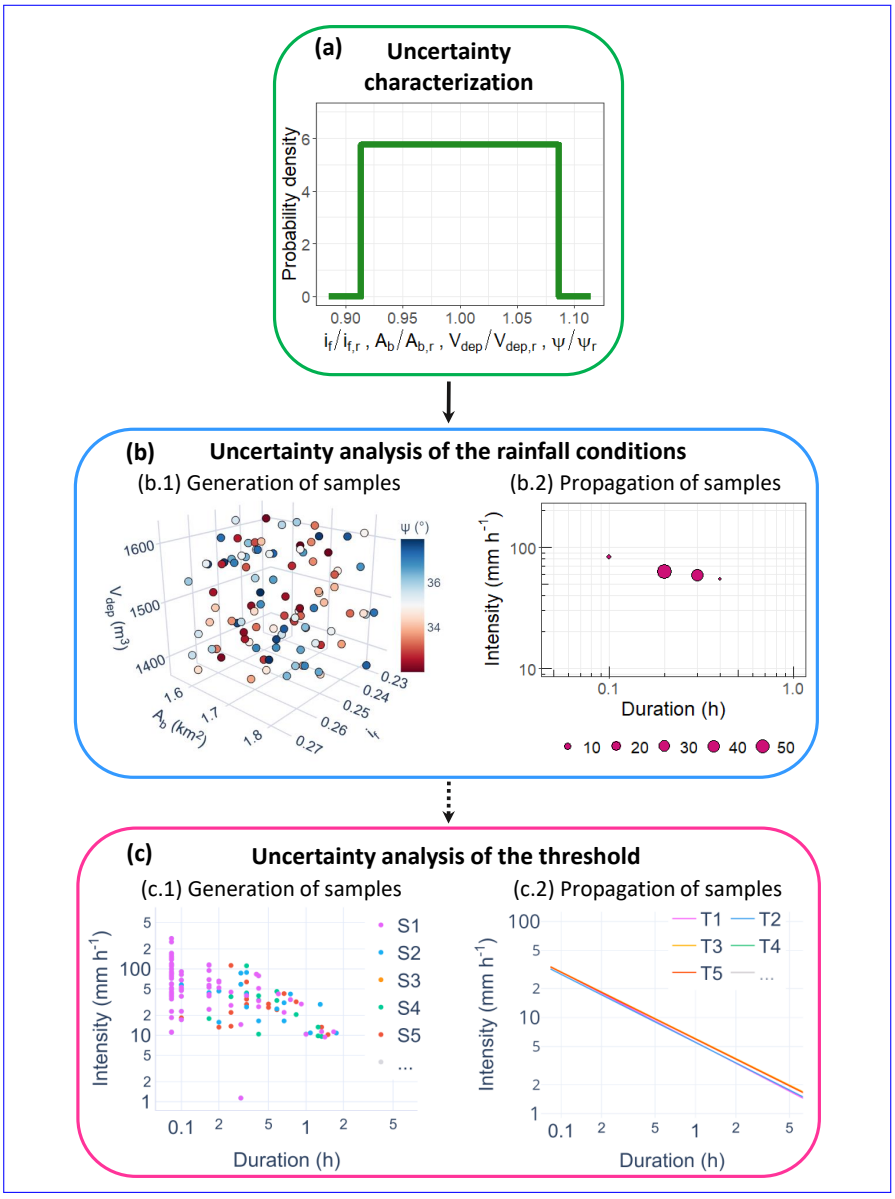

Figure 3. Scheme of the uncertainty analysis performed with Monte Carlo and Latin Hypercube Sampling method for the (I, D) couples computationtwo cascade MC simulations. For each event, the procedure consists of three steps. (a) Uncertainty characterization of the input parameters and data: the non-dimensional form of the input uncertain parameters and data, obtained by dividing the parameters variables by the reference value used in the calibration phase and indicated with a subscript $r$values, are assumed to be uniformly distributed. (b) Samples First MC simulation to compute the uncertainty analysis of the event characteristics for each debris flow: (b.1) samples generation performing the Latin Hypercube Sampling (LHS.) and (cb.2) Propagation propagation of samples through to compute the BDA method introducing the event hyetographcharacteristics. The dots size in the log-log ID plane indicates the absolute frequency of obtaining the (I, D) couples. (c) Second MC simulation to perform the uncertainty analysis of the threshold: (c.1) random samples S generation (one of the previous obtained (I, D) couples for each event) and (c.2) propagation of samples to estimate the thresholds T.

Table 1. Uncertainty probability Probability distributions of the input parameters established to perform the LHSuncertain variables for each event. $i_{f,r}$, $A_{b,r}$ and $V_{dep,r}$ are the event reference values (i.e. the values used in the calibration phase) of the average slope, of the basin area and of the deposited sediments respectively.

Input parameter/data Variable	Probability distribution function
i_f	Uniform$(i_{f,r}\,(1-5\%\,\sqrt{3}),\, i_{f,r}\,(1+5\%\,\sqrt{3}))$
A_b	Uniform$(A_{b,r}\,(1-5\%\,\sqrt{3}),\, A_{b,r}\,(1+5\%\,\sqrt{3}))$
V_{dep}	Uniform$(V_{dep,r}\,(1-5\%\,\sqrt{3}),\, V_{dep,r}\,(1+5\%\,\sqrt{3}))$
ψ	Uniform$(32°, 38°) \sim$ Uniform$(35°\,(1-5\%\,\sqrt{3}),\, 35°\,(1+5\%\,\sqrt{3}))$

4.2 Uncertainty analysis of the event characteristics

The procedure used to assess the propagation of the uncertainty in i_f, A_b, V_{dep} and ψ on the event characteristics (i.e. D, I, c and E) of each debris flow is schematized in Fig. 3(b) and it is composed of two main steps.

Fist, the input samples, namely the ordered sets of parameters variable values in the form $(i_f, A_b, V_{dep}, \psi)$, must be obtained. These samples are generated by using the LHS Latin Hypercube Sampling (LHS) (Fig. 3(b.1)), introduced by McKay et al. (2000). This method produces N samples starting with a division of each parameter variable uncertainty range into N disjoint intervals of equal probability. Then, one value is randomly selected within every interval, thus obtaining N values for each parametervariable. These values are then arranged in a matrixthe LHS matrix, composed of N rows and k columns, where k is the number of the parameters variables (four, in the specific case). In each column, the N values relevant to a single parameter variable are inserted in random order (Helton et al., 2006). Each row of this matrix gives one of the N parameter variable samples. According to Marino et al. (2008), to ensure the accuracy, the sample size N should be at least greater than k. In this study, N is set to 100 and the (100×4) LHS matrix is generated for each event, based on the previously established pdfs. Finally, the BDA outputs

Second, the event characteristics are obtained starting from each parameter input sample, resulting in 100 (I, D) couples for each event (Fig. 3(cb.2)), together with the related concentrations c and rainfall volumes per unit area E values, for each event.

The obtained results are then analysed in term of relative uncertainty, quantified through the computation of the CV of the output distributions. The CV, by definition, is a standardized measure of uncertainty (Håkanson, 2000) and allows to compare the relative variability of the results independently of their measurement units (Abdi, 2010) and of their means. For this reason, the CV is chosen as statistical measure to compare the relative variability between the outputs (between both the same output of different events and different outputs of the same event) and to understand how the uncertainty of an output variable changes depending on the event characteristics. In particular, the CVs are computed for all the BDA outputs.

Moreover, to evaluate how the Therefore, the overall total of (I, D) points move in the ID plane, the absolute uncertainty associated with the (I, D) couples estimation is quantified throughout the computation of the 95% uncertainty intervals. The extremes of the latter are defined as the 2.5 and 97.5 percentiles of the D and I distributions. The length of the uncertainty interval allows evaluating the absolute variability of the D and I distributions. couples obtained is $100 \cdot 84 = 8400$, where 84 is the number of considered debris flows.

4.3 Threshold uncertainty Uncertainty analysis of the threshold

To figure out the effects of the BDA outputs variability on the threshold computation, namely on the two constants a and b of Eq. (12), the uncertainties propagation is estimated The uncertainties propagation in the threshold estimate is quantified with a further Monte Carlo MC procedure. In this case, 5000 samples are a sample is generated selecting randomly one of the one hundred possible 100 (I, D) couples previously obtained for each event. The result is , resulting from the previous MC simulation (Fig. 3(c.1)). Hence, one sample consists of 84 (I, D) couples. Following this procedure, 5000 (a, b) couples, i. e. samples are created and used to estimate as many thresholds (Fig. 3(c.2)), namely 5000 different thresholds . (a, b) couples.

Consistently with the BDA output analysis, the relative uncertainty associated with the a and b distributions

5 Results and discussion

5.1 Variability of the event characteristics

As described in Sect. 4.2, the outputs of the first MC simulation applied to the dataset are 100 possible event characteristics (i.e. D, I, c and E) for each debris flow. The relative variability of all these outputs is quantified through the computation of the CV s. In addition, to analyse the threshold absolute uncertainty for each combination of threshold parameters, the intensity values are calculated for fixed durations selected within the threshold relevant time interval, from five minutes to six hours with a five minutes time step. In this way, for each duration we obtain an intensity frequency distributioncomposed of 5000 samples. Then, the 2.5 and 97.5 percentiles of these distributions are chosen as upper and lower bounds of the threshold uncertainty.

5.2 Comparison between MC outputs and reference values

In this analysis, we compare the MC means (I, D) couples, the threshold obtained with the mean values of a and b and of each event characteristic distribution. This allows providing a complete inspection and interpretation of the threshold uncertainty bounds with the results of the original calibration phase (reference values) in order to assess the differences between the two approachesall outputs. The absolute variability is then quantified through the computation of the variability range given by the difference between the minimum and the maximum values of the variable and it is evaluated only for the D and I distributions. This analysis allows highlighting the variability of the (I, D) couples in the ID plane for each event. Finally, possible correlations between the absolute variability and some event features are assessed.

As regards the rainfall conditions, according to Marra (2019), the bias of duration B_D and intensity B_I are computed for each event as:

$$B_D = \frac{D_m}{D_r} \qquad B_I = \frac{I_m}{I_r}$$

where the subscripts r and m represent respectively the reference value and the mean of the MC output distribution.

For what concerns the threshold, firstly the differences between the MC intensities $I_{MC,k}$, where k stands for mean, upper and lower bounds, and the reference threshold ones $I_{t,r}$ (Eq.) are carried out for the same fixed durations used to define the uncertainty bounds:

$$Diff = I_{MC,k} - I_{t,r}$$

Subsequently, the percentage changes, defined as:

$$\% \, change = \left(\frac{I_{MC,k} - I_{t,r}}{I_{t,r}} \right) \cdot 100$$

are computed to figure out how much the MC results deviate relatively from the calibrated threshold.

6 Results

5.1 Propagation of uncertainty in the BDA outputs

The method described in the previous section has been applied to the 84 debris flow events used to calibrate the threshold for the Trentino-Alto Adige/Südtirol region (Italy) in Rosatti et al. (2019).

5.0.1 Relative variability

The values of the CV, by definition, is a standardized measure of dispersion (Håkanson, 2000) and allows comparing the relative variability of the results independently of their measurement units (Abdi, 2010) and of their means. For this reason, the CV is chosen as the statistical quantity for comparing the relative variability between both the same characteristic of different events and different characteristics of the same event.

The CVs for the BDA outputs related to of the distributions of D, I, E and c for each event are shown in Table 2. The analysis of their variability allows to make the following observationsIn the following the trends and the differences in the CVs are highlighted and justified on the basis of some event aspects:

- D is the output characterised by distributions with the D distributions have the largest and most variable CVs with respect to all the other outputs. In fact, the events event characteristics: CV_D vary between 0% and 157.5%. The reason for this behaviour will be clarified further on;
- the distributions of I are characterised by a lower spread with respect to the D distributions, being all the CV_I values within 0% and to 30.0%. The reason of for this behaviour is connected to the fact that I, by definition, is an average and therefore the effects of the input parameters variability variables uncertainty are smoothed by the mean operatoraveraging. Also the reason why CV_I can be zero will be explained further on;
- also the concentration distributions show a low spread. As c is characterised by an upper bound (i.e. $0.9\,c_b$), the CV_c is strictly related to the proximity of c_r to this maximum value and consequently, according to Eq. (2), to the value of $i_{f,r}$. As shown in Fig. 4, until the $i_{f,r}$ is less than about 0.3, the CV_c tends to go up by increasing the $i_{f,r}$ since c_r is sufficiently smaller than $0.9\,c_b$. Instead, if the $i_{f,r}$ is between about 0.3 and 0.4, the CV_c tends to decrease by increasing the $i_{f,r}$ as c reaches the maximum and it is equal to $0.9\,c_b$ for an increasing number of i_f samples. Finally, the CV_c becomes 0% if the $i_{f,r}$ is grater greater than about 0.4 as c is always equal to $0.9\,c_b$ independently from the values of the i_f samples:. However, even in the worst conditions in terms of variability, CV_c is small and reaches a maximum value of 14.3%;

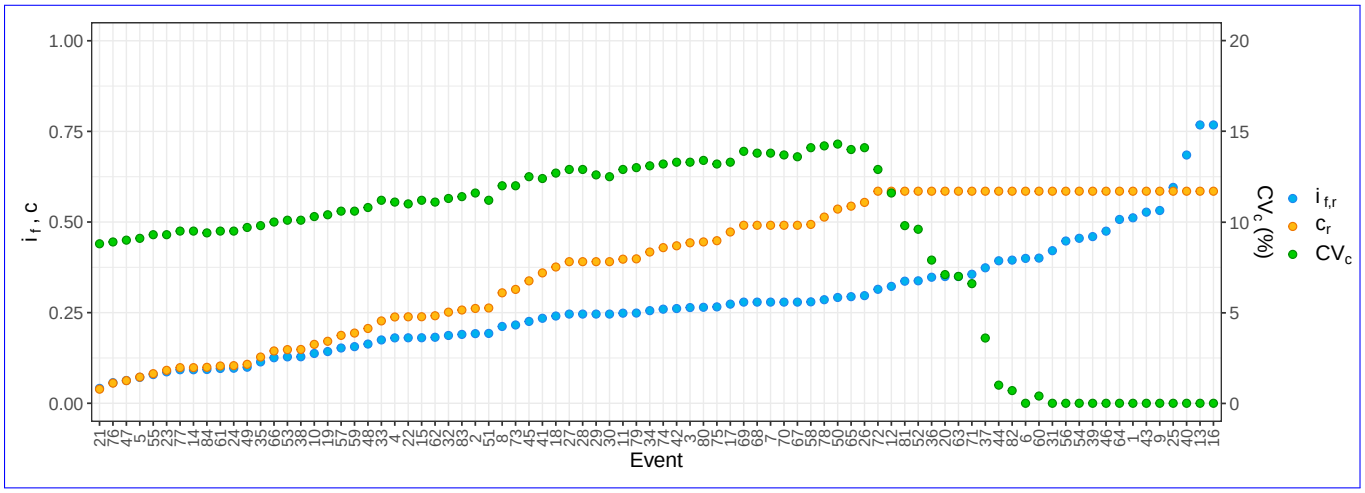

Figure 4. Comparison of the reference slope $i_{f,r}$, reference concentration c_r and CV_c trends. The events have been sorted with decreasing increasing slopes.

– the volume per unit area distributions shows CV_Es that vary between 7.1% and 64.6%. It is worth noting that high uncertainty in the estimation of E E does not necessarily imply large CV_D and/or CV_I (e.g. event 12) and vice versa (e.g. event 38). This suggests that the relative variability in I and D does not depend only on the relative variability in the needed rainfall volume per unit area but also on how the available rainfall volume is distributed into the hyetograph time intervals.

To better understand the variability of in D and I, we classify the events into three categories based on the CV_D values:

1. events with zero variability: $CV_D = 0\%$;
2. events with low variability: $0\% < CV_D \leq 30\%$;
3. events with high variability: $CV_D > 30\%$.

The first category comprises 48 events for which the 100 simulations of the MC method has provided as final outputs have provided always the same (I, D) couple. For these events, the propagation of the input parameters uncertainties does not effect variables uncertainty does not affect the (I, D) couple estimation resulting in $CV_D = CV_I = 0\%$. This type of result is related to two conditions:

– regardless of the input parameters variabilityvariables uncertainty, the concentration is always equal to $0.9\, c_b$. In this casealso the variation coefficient of the concentration , also CV_c is equal to zero (e.g. events 1, 13 and 25) and the variation of in E is only due to the propagation of the basin area and deposited volume uncertainties A_b and V_{dep} uncertainty (Eq. (4)), namely $CV_E \simeq 7.1\%$. For these 14 events, such a low small variation in E implies results in the constant computation of the same (I, D) couple;

Table 2. Coefficients of variation of the outputs of the BDA method event characteristics related to each event debris flow expressed as a percentage. CV_D is the coefficient of variation of the duration distribution, CV_I of the intensity distribution, CV_c of the concentration distribution and CV_E of the rainfall volume per unit area distribution.

Event	CV_D	CV_I	CV_c	CV_E	Event	CV_D	CV_I	CV_c	CV_E	Event	CV_D	CV_I	CV_c	CV_E
1	0.0	0.0	0.0	7.1	29	0.0	0.0	12.6	26.6	57	0.0	0.0	10.6	15.6
2	34.6	5.5	11.6	18.3	30	0.0	0.0	12.5	26.9	58	157.5	14.9	14.1	35.4
3	34.2	7.9	13.3	30.7	31	0.0	0.0	0.0	7.1	59	0.0	0.0	10.6	15.9
4	23.0	6.2	11.1	17.8	32	0.0	0.0	11.3	18.4	60	0.0	0.0	0.4	8.8
5	7.1	1.5	9.1	12.6	33	13.8	4.1	11.2	17.2	61	16.1	4.4	9.5	13.4
6	0.0	0.0	0.0	7.1	34	30.9	9.7	13.1	28.1	62	0.0	0.0	11.1	18.1
7	39.6	13.5	13.8	36.3	35	24.8	22.7	9.8	14.2	63	0.0	0.0	7.0	55.5
8	26.4	2.8	12.0	20.9	36	0.0	0.0	7.9	58.4	64	7.8	1.0	0.0	7.1
9	0.0	0.0	0.0	7.1	37	0.0	0.0	3.6	34.2	65	0.0	0.0	14.0	43.5
10	26.6	15.7	10.3	14.7	38	74.7	30.0	10.1	14.4	66	0.0	0.0	10.0	14.4
11	0.0	0.0	12.9	27.0	39	0.0	0.0	0.0	7.1	67	110.1	28.2	13.6	35.5
12	0.0	0.0	11.6	55.9	40	0.0	0.0	0.0	7.1	68	32.9	4.6	13.8	35.9
13	0.0	0.0	0.0	7.1	41	35.3	15.1	12.4	24.7	69	37.1	12.3	13.9	36.2
14	15.6	2.6	9.5	13.2	42	0.0	0.0	13.3	30.0	70	0.0	0.0	13.7	36.1
15	0.0	0.0	11.2	17.8	43	0.0	0.0	0.0	7.1	71	0.0	0.0	6.6	54.8
16	0.0	0.0	0.0	7.1	44	0.0	0.0	1.0	15.0	72	0.0	0.0	12.9	54.7
17	0.0	0.0	13.3	34.6	45	25.3	10.0	12.5	22.8	73	16.0	0.6	12.0	21.6
18	0.0	0.0	12.7	25.0	46	0.0	0.0	0.0	7.1	74	0.0	0.0	13.2	29.5
19	13.3	3.0	10.4	15.1	47	16.7	4.9	9.0	12.1	75	0.0	0.0	13.2	31.4
20	41.7	4.7	7.1	54.9	48	0.0	0.0	10.8	16.4	76	37.7	18.9	8.9	12.3
21	0.0	0.0	8.8	11.7	49	15.9	4.3	9.7	13.1	77	31.1	9.4	9.5	13.1
22	0.0	0.0	11.0	17.8	50	39.9	11.0	14.3	42.4	78	0.0	0.0	14.2	38.7
23	0.0	0.0	9.3	13.0	51	25.1	8.6	11.2	18.9	79	0.0	0.0	13.0	26.4
24	17.3	5.7	9.5	13.3	52	0.0	0.0	9.6	63.1	80	25.2	9.4	13.4	31.1
25	0.0	0.0	0.0	7.1	53	35.4	1.6	10.1	14.5	81	0.0	0.0	9.8	64.6
26	62.4	16.9	14.1	44.8	54	0.0	0.0	0.0	7.2	82	0.0	0.0	0.7	10.1
27	72.1	25.7	12.9	26.3	55	22.6	10.6	9.3	12.7	83	0.0	0.0	11.4	18.4
28	0.0	0.0	12.9	26.2	56	0.0	0.0	0.0	7.1	84	16.1	1.0	9.4	13.2

– despite CV_c is not zero and the CV_E is greater than 7.1% (e.g. event 28), the condition of Eq. (8) is satisfied, in all the 100 simulations, with the same time instants of the hyetograph considering always the same hyetograph time intervals. 34 events fall into this condition.

The For the 19 events that belong to the second categoryare characterised by I and D distributions relatively low spread around their mean values. For each of these 19 events, the uncertainty of the inputs implies the , the variables uncertainty results in the computation of more (I, D) couples which, however , that however are relatively close to the mean valuevalues: the I and D distributions are characterised by a standard deviation much smaller than the mean.

The third category includes 17 events for which the input parameters uncertainties propagation results in high relative uncertainty in the (I, D) couples computations. In general, these events are related to a hyetograph characterised by an intensity peak and low values around it. This sharp decrease in intensity implies thatsmall variations in E require large variations in the time intervals in order to satisfy variables uncertainty implies high values of CV_D. This means that, for these events, the number of time intervals needed to satisfy the condition of Eq. (8) . Event 58 is the extreme case of this condition: the duration vary greatly with respect to the mean number: the variables uncertainty has a relative great impact on the computation of D. Moreover, the highest values of CV_D highlight the presence of extremes in the D distribution, namely of values of D very distant from the mean. Indeed, CV is very sensitive to the extremes (e.g. Chau et al., 2005; Arachchige et al., 2020) , mainly if they are located in the right-hand tail of the distribution (Bendel et al., 1989). For instance, the effect of the extremes on the CV_D is evident in event 58: the D distribution of this event has an extreme much greater than the mean value (Fig. ??)5(a)). This is due to the presence of zero intensity temporal instants in the middle of the precipitation event hyetograph that must be considered (for two out of a hundred samples) to reach the higher highest values of E . For this reason, for some combinations of the input parameters, D is much greater than the mean value and these extremes entail an increase in the standard deviation , namely in (Fig. 5(b)). This results in a high value of the standard deviation with respect to the mean, namely a high value of the CV_D. The It is worth noting that the effects of this condition on I are fewer smaller thanks to the mean computation carried out to obtain this output. event characteristic.

As regards the absolute uncertainty associated with the (I, D) couples estimation, the results

5.0.2 Absolute variability

The absolute variability ranges in the ID plane of the (I, D) couples for each event allows us to get an idea of how variable an event as a whole is and to presume how this variability may affect the threshold estimate. Consistently with the relative variability, the events with $CV_D = CV_I = 0\%$ have also zero-length absolute variability ranges. The non-zero ranges are shown in Fig. 6: the horizontal and vertical lines represent respectively the 95% uncertainty intervals related to D and I. As evident, the length of the intervals ranges varies greatly depending on the event. In term of intensity, the maximum length is 61.3 66.21 mm h^{-1} and it is reached with the event 67 while, for the duration, the event 38 is characterised by the maximum length that is equal to 3.51 h. 5.25 h. Besides, the length of the range for D is less than 1 h in all but 8 events while for I it is less than 20 mm h^{-1} in all but 7 events. Moreover, in most cases, the mean is located neither vertically nor horizontally in the middle of the variability ranges, namely the D and I distributions are asymmetrical. To quantify the asymmetry of the I and D distributions, the related skewness SK_D and SK_I are computed for each event and shown in Fig. 7. The events with zero variability are

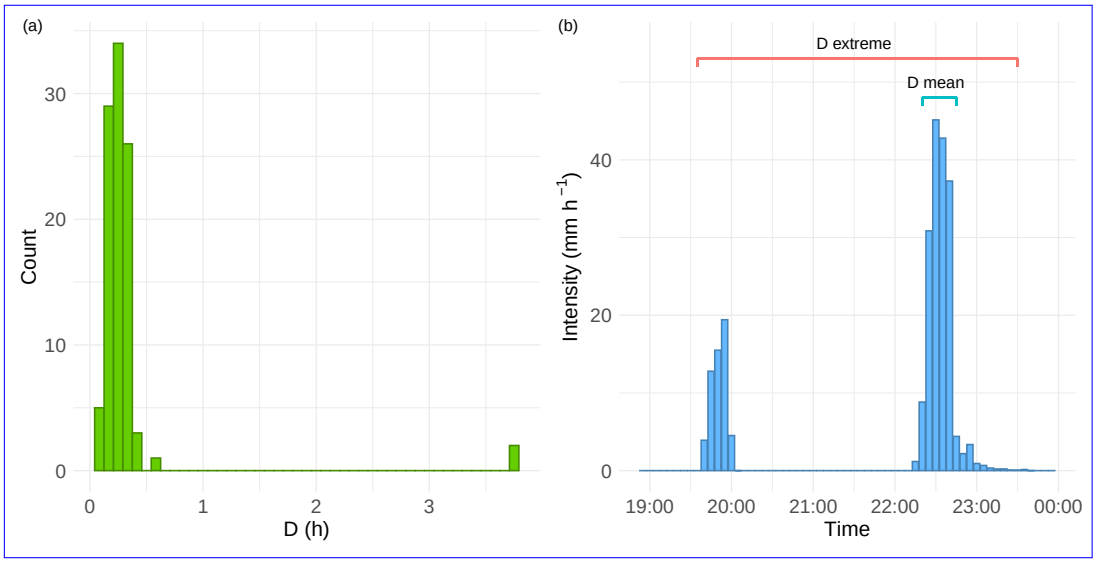

Figure 5. Hyetograph (a) Duration distribution histogram and (b) hyetograph of the event 58. In term The histogram shows the presence of D, an extreme isolated from the mass of the distribution. This extreme value (3.75 $D = 3.75$ h) is much greater than shown in the hyetograph and compared with the mean (0.32 $D = 0.32$ h).

characterised by $SK_D = 0$ and $SK_I = 0$. Moreover, in most cases, SK_D are positive while SK_I are negative: the longest tail of the distributions of D and I tends to be located on the right and the left of the mean respectively. This suggests that, given an event, the majority of the D values are characterized by duration shorter than the mean and the greatest contribution to the absolute variability is given by the longest durations (i.e. by the D distribution right extremes) as in event 38. Consistently, comparing Fig. 7 and Table 2, the events with the highest positive SK_D are the events with the highest CV_D (e.g. events 58 and 67). Instead, given an event, the concentration of the intensity values is greater towards the highest values and the smallest intensities (i.e. the I distribution left extremes) mostly contribute to the absolute variability (e.g. event 20 and 73). However, as said before, the I extremes have a slight impact on the absolute variability of I thanks to the mean procedure necessary for its computation that reduces the interval ranges.

5.1 Uncertainty in threshold computation

The main statistical quantities concerning the output a and b parameters distributions are given in Table 3. In particular, the variation coefficients are respectively 6.46% and 2.91%. These lowvalues highlight that the relative uncertainties associate to

5.0.1 Correlation between the absolute variability and some event features

Despite the specificity of each considered event, it's possible to identify some event features that are correlated with the D and I absolute variability. It is worth noting that, in general, correlation does not imply causation (Wiedermann and Von Eye, 2016) but it is a starting point to understand if causality between the variables can be established.

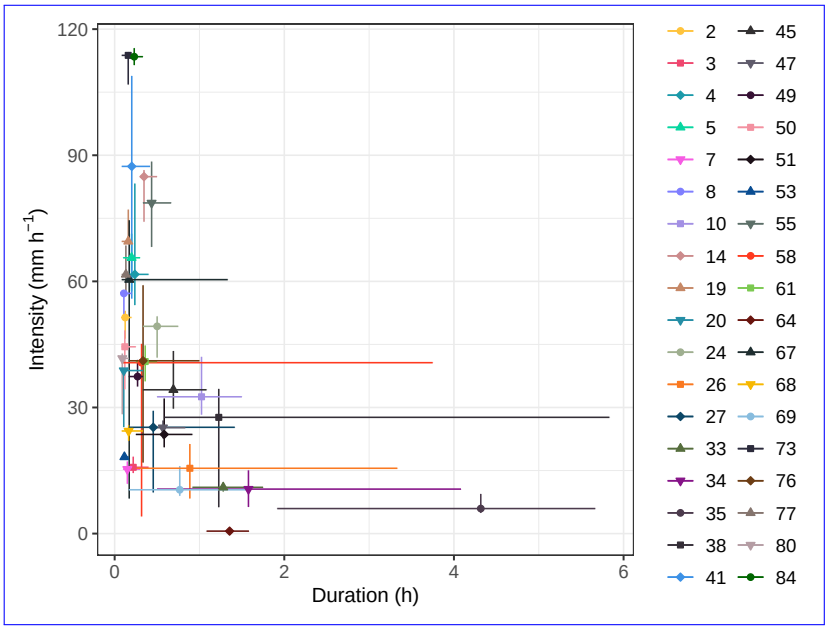

Figure 6. Plot of the uncertainty absolute variability in the (I, D) evaluation obtained with the Monte Carlo simulationscouples. The dots symbols are the mean values and the horizontal and vertical lines are respectively the duration and intensity absolute uncertainties (ivariability ranges. e. the 2.5 and 97.5 percentiles). To make the graph clearer, the points events with uncertainty intervals equal to zero have not been represented and the linear scale is used for both axis.

We define E_{av} as the rainfall volume per unit area available in the "main part of the hyetograph", namely the integral of the rainfall intensity on the smallest time interval comprising the peak and included between two instants with null intensities. We can then introduce the ratio E_r/E_{av}. As shown in Fig. 8, the absolute variability of D and E_r/E_{av} are positive correlated. A small value of E_r/E_{av} means that the main part of the hyetograph is amply able to provide E_r (i.e. to satisfy the condition of Eq. (8) in the reference conditions). This tends to avoid having to consider null intervals to achieve the values of E resulting from the MC simulation, namely to avoid D extremes. The opposite situation occurs if the ratio takes high values.

Regarding the intensity, we define I_{max} as the hyetograph maximum intensity and I_{mean} as the the mean intensity of the main part of the hyetograph for each event. The ratio I_{max}/I_{mean} provides a quantitative measure of the shape of the event hyetograph or, equivalently, of how much impulsive the event is. As shown in Fig. 9, a positive correlation subsists between the non-zero absolute variability of I and I_{max}/I_{mean}. If the shape of the hyetograph around the peak is flat, and the ratio I_{max}/I_{mean} is low, the variability of I, connected to the variability of D, is small since the average procedure, necessary to compute I, involves similar intensities intervals. The opposite occurs when the event is impulsive and the ratio is high. This consideration is valid only for events with non-zero absolute variability in I and D and tends to explain why some events with high variability in D have small variability in I (e.g. event 26).

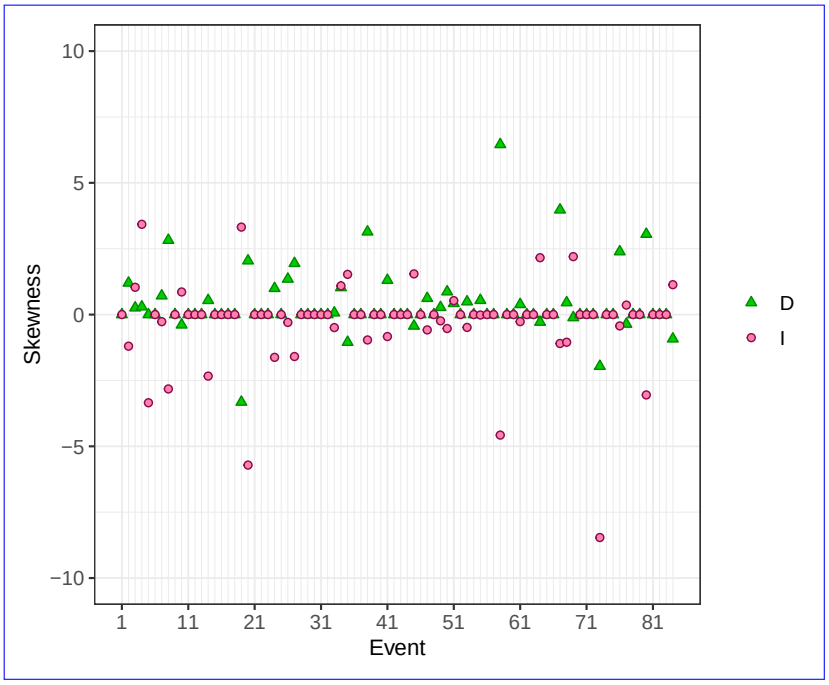

Figure 7. Skewness of the distributions of D and I for each event.

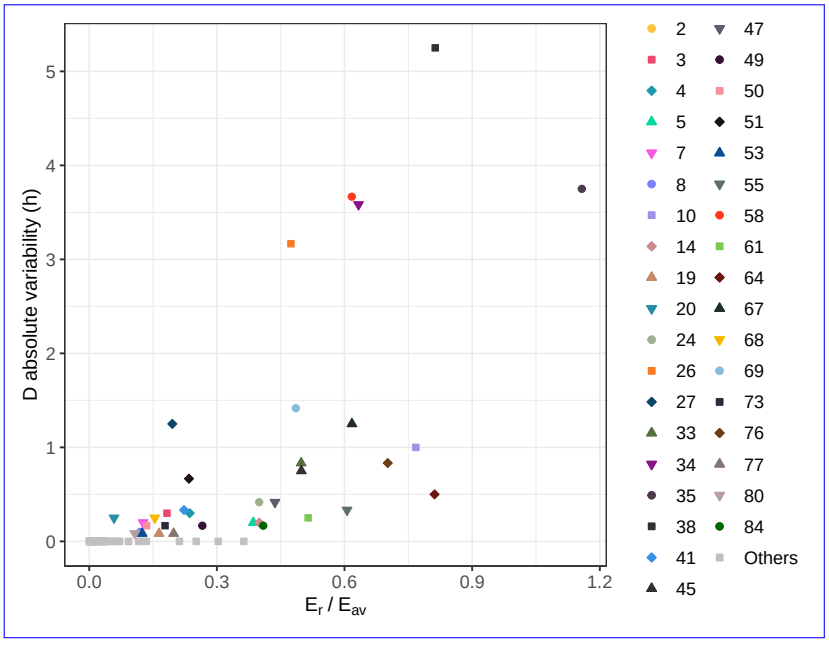

Figure 8. Positive correlation between the absolute variability of D and E_r/E_{av}, where E_{av} is the rainfall volume per unit area available in the main part of the hyetograph. Spearman correlation coefficient equals to 0.82 ($p < 2.2 \times 10^{-16}$). To make the graph clearer, the events with absolute variability of D equals to zero are represented with the same symbol.

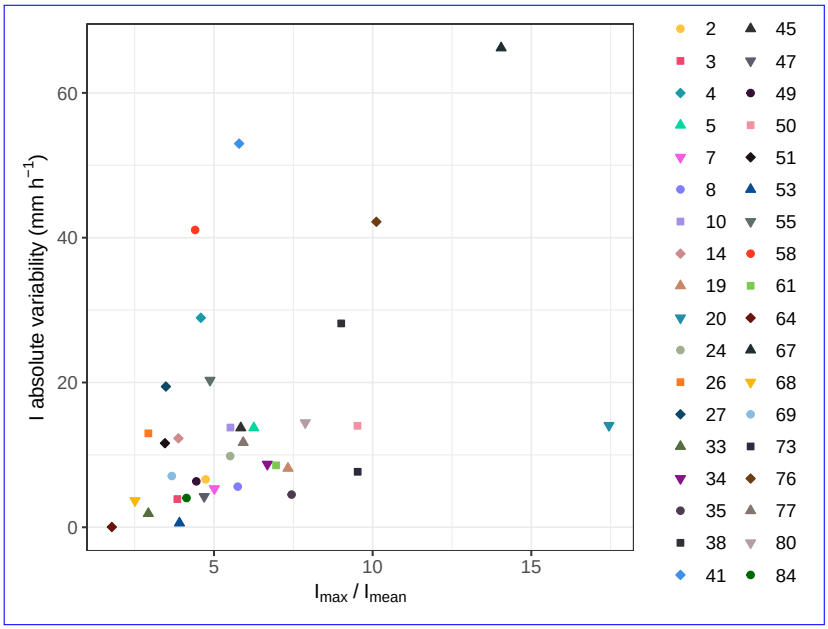

Figure 9. Positive correlation between the non-null absolute variability of I and I_{max}/I_{mean}. I_{max} is the maximum intensity and I_{mean} is the mean intensity of the main part of the hyetograph. Spearman correlation coefficient equals to 0.48 ($p = 0.0035$).

Table 3. Mean, standard deviation, variation coefficient CV and mean 95% confidence interval CI of the parameter coefficients a and b of Eq. (12), computed performing the Monte Carlo simulationssecond MC simulation.

Parameter Coefficient	Mean	Standard deviation	CV (%)	95% mean confidence interval
a	6.0056	0.3882	6.46	0.0108
b	0.6834	0.0199	2.91	0.0006

5.1 Variability of the threshold

The result of the second MC simulation is 5000 (a, b) couples. The main statistical quantities of their distributions are given in Table 3. The relative variability is quantified through the CV that is equal to 6.46% for a and 2.91% for $b$are very small. The low spread nature of the thresholds parameters a and b, highlighted by the small CV values, is also evident in the scatter plot and in the bivariate $3D$ histogram, respectively shown in Fig. 10(a) and 10(b).

Moreover, the lower and upper bounds of the threshold uncertainty, evaluated as explained in Sect. 4.3, are In addition, to analyse the absolute variability of the I-D threshold relation, the intensity values for each (a, b) couple are calculated for D values spanning from five minutes to six hours with a five minutes time step. In this way, for each duration, we obtain an intensity distribution composed of 5000 samples. Then, the 2.5 and 97.5 percentiles of these distributions are chosen as upper and lower bounds of the threshold absolute variability. The result is shown in Fig. 11. The uncertainty area is substantially symmetric to the According

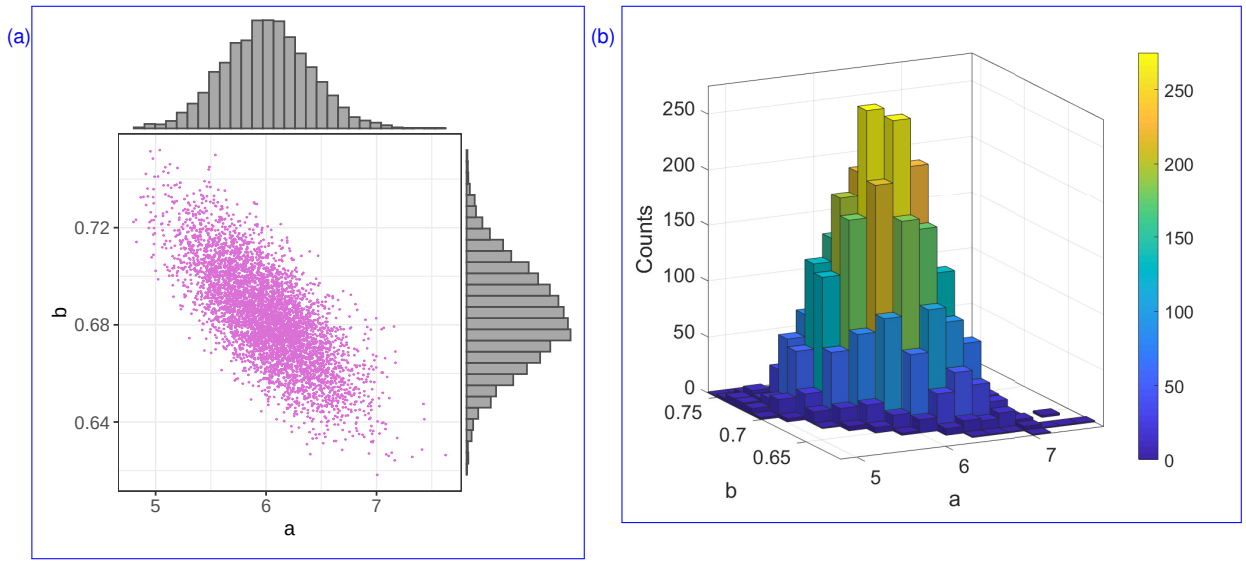

Figure 10. Values a and b of Eq. (12) obtained performing 5000 MC simulations: (a) scatter-plot and histogram and (b) $3D$ histogram

Values a and b of Eq. (12) obtained performing 5000 MC simulations: (a) scatter-plot and $2D$ histogram and (b) bivariate $3D$ histogram

to the substantially symmetrical distributions of a and b (Fig. 10(a)), the threshold computed with the mean values of the distributions of a and b (Table 3) . The is essentially equidistant from the lower and upper bounds. The variability bandwidth decreases monotonically by increasing the duration and varies between 5.61 mm h^{-1} and 0.64 mm h^{-1}. This means that the highest absolute uncertainties are related to shorter durations.

5.2 MC means and reference values

As regards the events rainfall condition, the biases between the reference values

Hence, both the relative and the absolute variability highlight that the effect of the uncertainty in the variables on the threshold estimate is small. This is mainly due to the zero variability in the D and the MC output distributions means (I distributions of 48 events out of 84: since the (I, D) points of these events are located in the same positions in all the 5000 MC simulations, they propagate zero uncertainty in the threshold computation.

5.2 Reference values versus MC means

Finally, a comparison between the results of the first and second MC simulation and the reference values is carried out. In particular, we compare:

- the means of the D and I distributions (Fig. 6), obtained with the first MC simulation, to the corresponding reference ones, for each event;

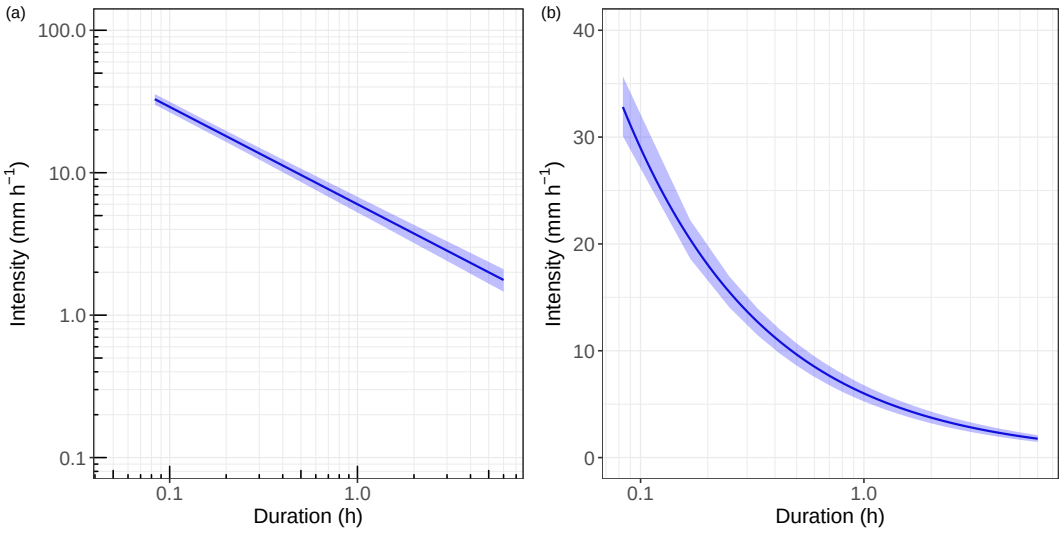

Figure 11. (a) Log-log and (b) semi-log plot of the threshold absolute uncertainty variability. The blue line is the rainfall threshold obtained using the mean value of a and b (Table 3). The shaded area represents the threshold uncertainty absolute variability whose upper and lower bounds have been computed considering the 2.5 and 97.5 percentiles of the intensity distributions for fixed durations.

– the mean threshold (i.e. threshold computed with the mean values of a and b) and the threshold absolute variability bounds (Fig. 11), resulting from the second MC simulation, to the reference threshold (i.e. Eq. (14))are 13)).

As regards D and I, according to Marra (2019), the bias of duration B_D and intensity B_I are computed for each event as:

$$B_D = \frac{D_m}{D_r} \qquad B_I = \frac{I_m}{I_r} \tag{14}$$

where the subscripts m represent the mean of the MC D and I distributions. The result is shown in Fig. 12. : B_D deviates between 0.8 and 1.5 (Fig. 12(a)) while B_I between 0.86 and 1.15 (Fig. 12(b)). Consistently with the analysis of the CV variability analysis described in Sect. 5.1, most events (48) are characterised by $B_D = B_I = 1$. This means that for these zero-variability events, the reference duration and intensity are exactly the MC mean values of I and D, namely the only MC (I, D) couple. Moreover, most of the remaining events have $B_D > 1$ and $B_I < 1$:. This signifies that the MC (I, D) mean couples tend to be located lower and more to the right than the reference ones . This condition highlights an underestimation of some mean rainfall conditions with respect to the reference onesin the log-log ID plane.

As regards Regarding the threshold, the differences between the mean, lower and upper bounds MC intensities and MC intensities $I_{MC,k}$, where k stands for mean, upper bound and lower bound, and the reference threshold ones (Eq. (15)) as a function of D are $I_{t,r}$ are carried out for the same durations used to define the absolute variability of the threshold:

$$\mathrm{Diff}(k, D) = I_{MC,k}(D) - I_{t,r}(D), \quad k = \text{mean, upper bound, lower bound} \tag{15}$$

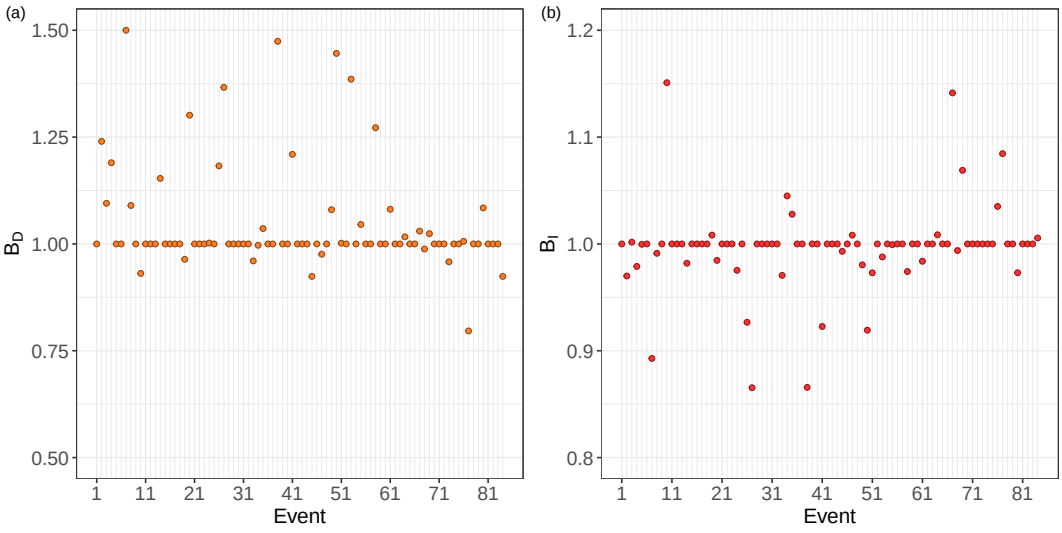

Figure 12. Bias of (a) duration B_D and (b) intensity B_I between the mean values of the variable D and I distributions obtained performing the first MC simulations simulation and the corresponding reference values for each event.

The result is shown in Fig. 13(a). For almost all durations, the threshold obtained with the MC mean values of a and b is intensities of the mean threshold are slightly lower than the reference onethreshold ones: a positive difference occurs only for the first time interval. Consistently with the obtained a and b mean values (Table 3) and the B_D and B_I trends, in the log-log ID plane the mean threshold is respectively slightly more downward translated and clockwise rotated than the reference one. Instead, the upper and lower bounds are respectively always higher and lower than the reference threshold. This means that the latter is contained in the MC threshold uncertainty area. This behaviour is also evident

Subsequently, the percentage changes, defined as:

$$\%\,\text{change}\,(\text{k},\text{D}) = \left(\frac{\text{Diff}\,(\text{k},\text{D})}{\text{I}_{\text{t,r}}\,(\text{D})}\right)\cdot 100, \quad \text{k} = \text{mean, upper bound, lower bound} \tag{16}$$

are computed to figure out how much the second MC outcomes deviate relatively from the reference threshold. The percentage changes are plotted in Figure 13(b)where the percentage changes (Eq. (16)) are plotted: the mean threshold deviates between 0.14% and -5.44%, the upper bound between 8.06% and 12.31% and the lower bound between -8.34% and -22.94% from the reference one.

This study aimed to figure out the effect It can therefore be generally stated that the outcomes of the uncertainty of some parameters on the computation of BDA outputs and on the subsequent threshold calibration. In summary, analyses, both (I, D) couples and threshold estimate, are consistent with the reference ones. Coherently with the previous analysis, also in this comparison, the duration is the quantity with the highest bias values. However, the mean threshold and the results obtained for the BDA outputs analysishas highlighted that the uncertainty of the inputs may result in a both low and high variation of the outputs distributions depending on the event characteristics and on the variable considered. The main uncertainties are related to the computation of D, as evident from Table 2 and Fig. 6, and are mainly due to the piecewise constant nature and shape of the hyetograph. Indeed, given

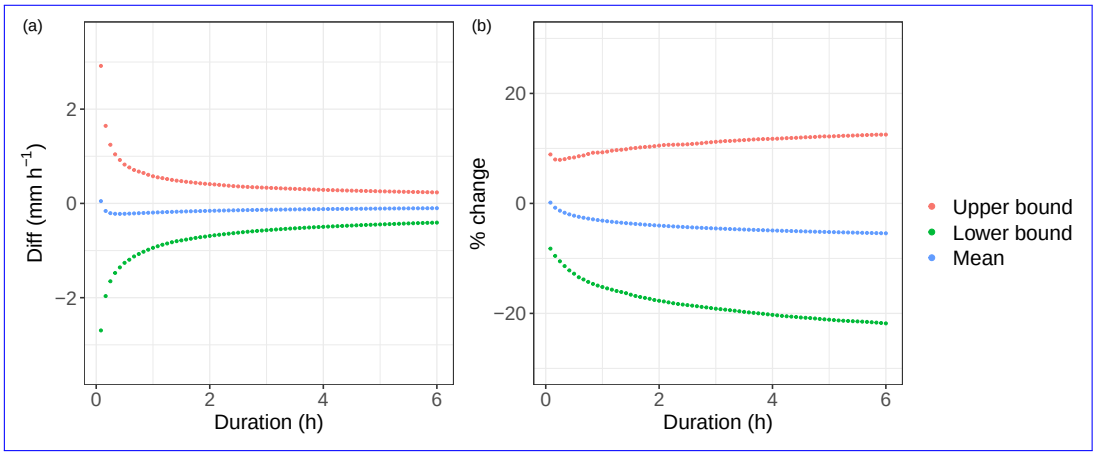

Figure 13. (a) Difference between the MC intensities (upper bound, lower bound and values obtained with the meanvalues of a and b) and the reference threshold ones as a function of the duration; (b) percentage change of the MC intensities respect the reference threshold ones, as a function of the duration.

the discrete nature of $i(t)$, in some cases, even a small change in E may result in a relatively large variation of D (e.g. event 38), namely in the number of temporal instants necessary to achieve the needed rainfall volume. This is especially true if the hyetograph is characterized by time intervals with zero intensity within the event. However, although some events are characterised by a high uncertainty in the estimation of the (I, D) couple, the threshold computation is not affected by high variability. Both the threshold parameters have low variation coefficient (Table 3), are low spread within the ab plane (Fig. 10) and the upper and lower bounds of the uncertainty area are close to reference one are very close, pointing out the small effects of the differences between D_m and D_r on the threshold computation.

5.3 Further elements of uncertainty

In the calibration of the BDA-based threshold and in the assumptions of the developed method used to assess the uncertainty, it is possible to identify some elements that may introduce further uncertainty, beyond that considered in this analysis, in the calculation of the event characteristics and, consequently, in the estimate of the mean threshold (Fig. 11). This low uncertainty is mainly due to zero variability of 48 events outputs: since the (I, D) points of these events are located in the same positions in all the 5000 MC simulations, they propagate zero threshold. Firstly, the variability ranges and the probability distributions of the parameters and data, namely the uncertainty characterisation of the variables, are uncertain. Secondly, the equations of the BDA may be uncertain since they are based on some simplifications and hypothesis. Finally, the radar data may be affected by uncertainty due to other sources of error, beyond the beam shielding one (considered in this analysis), such as signal attenuation in heavy rain or wet radome attenuation (Marra et al., 2014). Nevertheless, at the present state of the research, it is not possible to assess the impact of these uncertainties on the event characteristics estimate and further study is required.

6 Conclusions

This study has aimed to assess the effects of the uncertainty in the threshold computation. Moreover, physical and morphological parameters and data on the BDA-based threshold calibration to evaluate the method robustness. To that end, a suitable methodology composed of two MC cascade simulations has been developed and applied to a specific study area and dataset. The first MC simulation has allowed examining the uncertainty propagation in the event characteristics estimate. The results have highlighted that the (I, D) couples can be affected by both high and low variability. Overall, the duration has found to be the most variable outcome in relative term while I, thanks to the average procedure, has a lower relative variability. In absolute term, the variability of the deviation between the MC results and the reference values has been analysed both in term of (I, D) couple estimation and threshold computation. As evident from Fig.12, most events are characterised by B_D and B_I equal or close to 1. However, the duration bias of some events is high. Despite this, the reference threshold is very close to the threshold computed with couples differs greatly between the events and the MC mean value of a D and b and is contained in the uncertainty area (Fig. 13). This means that if the uncertainty analysis has been done during the calibration of the I distributions tend to be skewed to the right and left respectively. Moreover, considering the mean values of the events with non-zero variability (36 events out of 84), the uncertainty in the variables tends to provide slightly longer durations and slightly smaller intensities with respect to the reference ones. Notwithstanding, the second MC simulation has shown that the threshold computation is affected by small variability. The low dispersion of the threshold coefficients is mainly due to the 48 events with zero variability. As a result, the BDA method, applied to the considered dataset, can be described as robust since it provides a calibrated threshold low sensitive to the considered uncertainty in the parameters and data. This is also highlighted from the consistency between the uncertainty analysis mean threshold and the mean threshold had been accepted, there would have been no large variationsreference one.

As evident, the most critical part of the study is the computation of the (I, D) couples. High variability of some I Overall, the results of this analysis can be useful to calibrate a BDA-based threshold for a different study area since the investigation has highlighted the main critical elements that could undermine the BDA robustness. In particular, given a debris flow and the related rainfall event, it was noted that some event features are correlated with the variability of D and I. The percentage of needed rainfall volume and available one in the main part of the hyetograph is positive correlated with the absolute variability of D. Moreover, the shape of the main part of the hyetograph, described by the ratio between the maximum and the mean intensity, is positive correlated with the non-null absolute variability of I. Therefore, given an event, these trends can be used to presume the possible variability in the estimate of D output distributions points out the presence of possible critical issues in the estimation of the rainfall conditions associated with the event, as also highlight in Rosatti et al. (2019). The critical issues may be due to three main conditions. Firstly, some combinations of the input parameters, obtained with the LHS method, may be not representative of the analysed event. This condition leads to inconsistent estimates of the rainfall volume and and I, consequently, of without carrying out a specific uncertainty analysis. In other words, if an event is characterised by (i) low availability of rainfall volume in the main part of the hyetograph with respect to the needed one and (ii) a peak intensity much greater than the mean one, variations in the the parameters and data is likely to result in high variability in D and I . Secondly, the analysed debris flow may have had a different dynamic than the simplified one on which the BDA is based. For instance, the hypothesized equilibrium condition may have not been reached by some events due to particular conditions, such as lack of sediments, the presence of non-erodible zones or initiation of a debris flow caused by slope failure. This leads to an overestimation or underestimation of the concentration and , therefore, to a not reliable rainfall condition estimation. Finally, according to Marra et al. (2014), the radar data may be affected by some sources of error. During the calibration phase, to avoid the source of error related to the beam shielding, typical phenomenon for mountain regions (Germann et al., 2006),

estimate. The presence of many events of this type could undermine the BDA robustness. Therefore, in these cases, it is advisable to put care in the estimate of the events have been filtered out based on the radar signal power. Events with radar signal weakened more than 90% have been excluded (Rosatti et al., 2019). However, other sources of error, such as signal attenuation in heavy rain or wet radome attenuation, have not been considered in the current study. If present, these errors propagate in the computation of V_r^{DF} (Eq. (8)) implying an over or underestimation of the available rainfall volume. This results in a wrong estimate of the event (I, D) couple. parameters and data.

Besides, given an event, further elements likely affecting the estimate of event characteristics have been highlighted in this study: (i) the variability ranges and probability distributions of the parameters and data, (ii) the equations constituting the BDA model and (iii) radar data. These elements can be affected by uncertainty and impact the event characteristics estimate. The uncertainty analysis performed in this study does not provide quantitative information on these impacts. Further analysis will assess how these three conditions elements affect the (I, D) couple estimation estimate and, consequently, the threshold calibration.

However, the BDA methodseems to be robust enough to provide a reliable rainfall threshold : the input parameters uncertainties result in a low variation of the threshold estimation. Further analysis will also assess the robustness and the reliability Moreover, the developed method, composed of two cascade MC simulations, can be applied to assess the uncertainty related to other threshold calibration approaches whose event characteristics estimate is based not only on the hyetograph but also on other variables (e.g. the one proposed by Zhang et al. (2020)). Indeed, the developed method allows considering the entire range of uncertainty of the variables and, therefore, avoiding the analysis by scenarios, quite widespread in the literature for the uncertainty analysis of rainfall thresholds (e.g. Nikolopoulos et al., 2014; Peres et al., 2018). Analysing by scenarios may not be suitable if the uncertain parameters have a continuous range of variability. Indeed, a low number of input values combinations may not provide an overall assessment of the variability of the outputs.

Finally, it is worth noting that the results of this analysis are not useful to check the forecast capability of the thresholdto forecast the possible occurrence of debris flow. Indeed, the variability in the threshold estimate due to the uncertainty of the inputs is not related to its forecast effectiveness but only to its robustness. The threshold forecast capability can be proved only by performing a proper validation analysis, essential to make this tool operational. Since the calibration method applied to the specific study area is proved to be robust, further analysis will assess the forecast capability of the threshold, developing an appropriate validation method.

Author contributions. MM designed the experiments, performed the analysis and wrote the paper. DZ and GR supervised the study, analysed the results and wrote the paper.

Competing interests. The authors declare that they have no conflict of interest.

Acknowledgements. This work has been carried out within the project "Progetto WEEZARD: un sistema integrato di modellazione matematica a servizio della sicurezza nei confronti di pericoli idrogeologici in ambiente montano" (CARITRO Foundation – Cassa di Risparmio di Trento e Rovereto). We thank Prof. Siboni for providing valuable suggestions and Ripartizione Opere Idrauliche and Ufficio Idrografico, Provincia Autonoma di Bolzano (Italy) and Servizio Bacini Montani and Ufficio Previsioni e Pianificazione, Provincia Autonoma di Trento (Italy) for supplying radar and debris flow debris-flow data.

References

Abdi, H.: Coefficient of variation, Encyclopedia of research design, 1, 169–171, 2010.

Abraham, M. T., Satyam, N., Rosi, A., Pradhan, B., and Segoni, S.: The Selection of Rain Gauges and Rainfall Parameters in Estimating Intensity-Duration Thresholds for Landslide Occurrence: Case Study from Wayanad (India), Water, 12, 2020.

Aleotti, P.: A warning system for rainfall-induced shallow failures, Engineering Geology, 73, 247 – 265, Rainfall-triggered landslides and debris flows, 2004.

Arachchige, C. N., Prendergast, L. A., and Staudte, R. G.: Robust analogs to the coefficient of variation, Journal of Applied Statistics, pp. 1–23, 2020.

Baum, R. L. and Godt, J. W.: Early warning of rainfall-induced shallow landslides and debris flows in the USA, Landslides, 7, 259–272, 2010.

Bendel, R., Higgins, S., Teberg, J., and Pyke, D.: Comparison of skewness coefficient, coefficient of variation, and Gini coefficient as inequality measures within populations, Oecologia, 78, 394–400, 1989.

Bernard, M., Boreggio, M., Degetto, M., and Gregoretti, C.: Model-based approach for design and performance evaluation of works controlling stony debris flows with an application to a case study at Rovina di Cancia (Venetian Dolomites, Northeast Italy), Science of the total environment, 688, 1373–1388, 2019.

Bisci, C., Fazzini, M., Dramis, F., Lunardelli, R., Trenti, A., and Gaddo, M.: Analysis of spatial and temporal distribution of precipitation in Trentino (Italian Eastern Alps): Preliminary Report., Meteorologische Zeitschrift, pp. 183–187, 2004.

Blijenberg, H.: In-situ strength tests of coarse, cohesionless debris on scree slopes, Engineering Geology, 39, 137–146, 1995.

Brardinoni, F., Church, M., Simoni, A., and Macconi, P.: Lithologic and glacially conditioned controls on regional debris-flow sediment dynamics, Geology, 40, 455–458, 2012.

Brunetti, M., Peruccacci, S., Rossi, M., Luciani, S., Valigi, D., and Guzzetti, F.: Rainfall thresholds for the possible occurrence of landslides in Italy, Natural Hazards & Earth System Sciences, 10, 2010.

Caine, N.: The rainfall intensity-duration control of shallow landslides and debris flows, Geografiska annaler: series A, physical geography, 62, 23–27, 1980.

Cánovas, J. B., Stoffel, M., Corona, C., Schraml, K., Gobiet, A., Tani, S., Sinabell, F., Fuchs, S., and Kaitna, R.: Debris-flow risk analysis in a managed torrent based on a stochastic life-cycle performance, Science of the total environment, 557, 142–153, 2016.

Cepeda, J., Höeg, K., and Nadim, F.: Landslide-triggering rainfall thresholds: a conceptual framework, Quarterly Journal of Engineering Geology and Hydrogeology, 43, 69–84, 2010.

Chau, T., Young, S., and Redekop, S.: Managing variability in the summary and comparison of gait data, Journal of neuroengineering and rehabilitation, 2, 1–20, 2005.

Chien-Yuan, C., Tien-Chien, C., Fan-Chieh, Y., Wen-Hui, Y., and Chun-Chieh, T.: Rainfall duration and debris-flow initiated studies for real-time monitoring, Environmental Geology, 47, 715–724, 2005.

Coleman, H. W. and Steele, W. G.: Experimentation, validation, and uncertainty analysis for engineers, John Wiley & Sons, 2018.

Dowling, C. A. and Santi, P. M.: Debris flows and their toll on human life: a global analysis of debris-flow fatalities from 1950 to 2011, Natural hazards, 71, 203–227, 2014.

Frattini, P., Crosta, G., and Sosio, R.: Approaches for defining thresholds and return periods for rainfall-triggered shallow landslides, Hydrological Processes: An International Journal, 23, 1444–1460, 2009.

Fuchs, S., Keiler, M., Sokratov, S., and Shnyparkov, A.: Spatiotemporal dynamics: the need for an innovative approach in mountain hazard risk management, Natural hazards, 68, 1217–1241, 2013.

Gariano, S. L., Melillo, M., Peruccacci, S., and Brunetti, M. T.: How much does the rainfall temporal resolution affect rainfall thresholds for landslide triggering?, Natural Hazards, 2020a.

595 Gariano, S. L., Melillo, M., Peruccacci, S., and Brunetti, M. T.: How much does the rainfall temporal resolution affect rainfall thresholds for landslide triggering?, Natural Hazards, 2020b.

Germann, U., Galli, G., Boscacci, M., and Bolliger, M.: Radar precipitation measurement in a mountainous region, Quarterly Journal of the Royal Meteorological Society: A journal of the atmospheric sciences, applied meteorology and physical oceanography, 132, 1669–1692, 2006.

600 Giannecchini, R.: Rainfall triggering soil slips in the southern Apuan Alps (Tuscany, Italy), Advances in Geosciences, 2, 21–24, 2005.

Giannecchini, R., Galanti, Y., Avanzi, G. D., and Barsanti, M.: Probabilistic rainfall thresholds for triggering debris flows in a human-modified landscape, Geomorphology, 257, 94–107, 2016.

Guzzetti, F., Peruccacci, S., Rossi, M., and Stark, C. P.: Rainfall thresholds for the initiation of landslides in central and southern Europe, Meteorology and Atmospheric Physics, 98, 239–267, 2007.

605 Guzzetti, F., Peruccacci, S., Rossi, M., and Stark, C. P.: The rainfall intensity–duration control of shallow landslides and debris flows: an update, Landslides, 5, 3–17, 2008.

Helton, J. C. and Davis, F. J.: Latin hypercube sampling and the propagation of uncertainty in analyses of complex systems, Reliability Engineering and System Safety, 81, 23–69, 2003.

Helton, J. C., Johnson, J. D., Sallaberry, C. J., and Storlie, C. B.: Survey of sampling-based methods for uncertainty and sensitivity analysis,

610 Reliability Engineering and System Safety, 91, 1175–1209, 2006.

Håkanson, L.: The role of characteristic coefficients of variation in uncertainty and sensitivity analyses, with examples related to the structuring of lake eutrophication models, Ecological Modelling, 131, 1 – 20, 2000.

Hofer, E.: The Uncertainty Analysis of Model Results, Springer International Publishing, 2018.

Huebl, J. and Fiebiger, G.: Debris-flow mitigation measures, in: Debris-flow hazards and related phenomena, pp. 445–487, Springer, 2005.

615 Iadanza, C., Trigila, A., and Napolitano, F.: Identification and characterization of rainfall events responsible for triggering of debris flows and shallow landslides, Journal of Hydrology, 541, 230–245, 2016.

Jakob, M., Owen, T., and Simpson, T.: A regional real-time debris-flow warning system for the District of North Vancouver, Canada, Landslides, 9, 165–178, 2012.

Lane, E. W.: Progress report on studies on the design of stable channels by the Bureau of Reclamation, in: Proceedings of the American

620 Society of Civil Engineers, vol. 79, pp. 1–31, ASCE, 1953.

Li, T.-T., Huang, R.-Q., and Pei, X.-J.: Variability in rainfall threshold for debris flow after Wenchuan earthquake in Gaochuan River watershed, Southwest China, Natural Hazards, 82, 1967–1980, 2016.

Marchi, L., Brunetti, M. T., Cavalli, M., and Crema, S.: Debris-flow volumes in northeastern Italy: Relationship with drainage area and size probability, Earth Surface Processes and Landforms, 44, 933–943, 2019.

625 Marino, S., Hogue, I. B., Ray, C. J., and Kirschner, D. E.: A methodology for performing global uncertainty and sensitivity analysis in systems biology, 2008.

Marra, F.: Rainfall thresholds for landslide occurrence: systematic underestimation using coarse temporal resolution data, Natural Hazards, 95, 883–890, 2019.

Marra, F., Nikolopoulos, E. I., Creutin, J. D., and Borga, M.: Radar rainfall estimation for the identification of debris-flow occurrence thresholds, Journal of Hydrology, 519, 1607–1619, 2014.

Marra, F., Nikolopoulos, E. I., Creutin, J. D., and Borga, M.: Space–time organization of debris flows-triggering rainfall and its effect on the identification of the rainfall threshold relationship, Journal of Hydrology, 541, 246–255, 2016.

McKay, M. D., Beckman, R. J., and Conover, W. J.: A comparison of three methods for selecting values of input variables in the analysis of output from a computer code, Technometrics, 42, 55–61, 2000.

Nikolopoulos, E. I., Crema, S., Marchi, L., Marra, F., Guzzetti, F., and Borga, M.: Impact of uncertainty in rainfall estimation on the identification of rainfall thresholds for debris flow occurrence, Geomorphology, 221, 286–297, 2014.

Oberkampf, W. L., Helton, J. C., Joslyn, C. A., Wojtkiewicz, S. F., and Ferson, S.: Challenge problems: uncertainty in system response given uncertain parameters, Reliability Engineering & System Safety, 85, 11–19, 2004.

Pan, H.-L., Jiang, Y.-J., Wang, J., and Ou, G.-Q.: Rainfall threshold calculation for debris flow early warning in areas with scarcity of data, Natural Hazards and Earth System Sciences, 18, 1395–1409, 2018.

Peres, D. J., Cancelliere, A., Greco, R., and Bogaard, T. A.: Influence of uncertain identification of triggering rainfall on the assessment of landslide early warning thresholds, Natural Hazards and Earth System Sciences, 18, 633–646, 2018.

Peruccacci, S., Brunetti, M. T., Luciani, S., Vennari, C., and Guzzetti, F.: Lithological and seasonal control on rainfall thresholds for the possible initiation of landslides in central Italy, Geomorphology, 139, 79–90, 2012.

Pisoni, E., Albrecht, D., Mara, T. A., Rosati, R., Tarantola, S., and Thunis, P.: Application of uncertainty and sensitivity analysis to the air quality SHERPA modelling tool, Atmospheric environment, 183, 84–93, 2018.

Prancevic, J. P. and Lamb, M. P.: Unraveling bed slope from relative roughness in initial sediment motion, Journal of Geophysical Research: Earth Surface, 120, 474–489, 2015.

R Core Team: R: A Language and Environment for Statistical Computing, R Foundation for Statistical Computing, Vienna, Austria, http://www.R-project.org/, 2013.

Rosatti, G., Zugliani, D., Pirulli, M., and Martinengo, M.: A new method for evaluating stony debris flow rainfall thresholds: the Backward Dynamical Approach, Heliyon, 5, 2019.

Rossi, M., Luciani, S., Valigi, D., Kirschbaum, D., Brunetti, M., Peruccacci, S., and Guzzetti, F.: Statistical approaches for the definition of landslide rainfall thresholds and their uncertainty using rain gauge and satellite data, Geomorphology, 285, 16–27, 2017.

Segoni, S., Piciullo, L., and Gariano, S. L.: A review of the recent literature on rainfall thresholds for landslide occurrence, 2018.

Staley, D. M., Kean, J. W., Cannon, S. H., Schmidt, K. M., and Laber, J. L.: Objective definition of rainfall intensity–duration thresholds for the initiation of post-fire debris flows in southern California, Landslides, 10, 547–562, 2013.

Stancanelli, L., Lanzoni, S., and Foti, E.: Propagation and deposition of stony debris flows at channel confluences, Water Resources Research, 51, 5100–5116, 2015.

Takahashi, T.: Mechanical characteristics of debris flow, Journal of the Hydraulics Division, 104, 1153–1169, 1978.

Takahashi, T.: A review of Japanese debris flow research, International Journal of Erosion Control Engineering, 2, 1–14, 2009.

Takahashi, T.: Debris flow: mechanics, prediction and countermeasures, CRC press, 2014.

Uijlenhoet, R.: Raindrop size distributions and radar reflectivity-rain rate relationships for radar hydrology, Hydrology and Earth System Sciences, 5, 615–627, 2001.

Wiedermann, W. and Von Eye, A.: Statistics and causality, Wiley Online Library, 2016.

Winter, M., Dent, J., Macgregor, F., Dempsey, P., Motion, A., and Shackman, L.: Debris flow, rainfall and climate change in Scotland, Quarterly Journal of Engineering Geology and Hydrogeology, 43, 429–446, 2010.

Zhang, S. J., Xu, C. X., Wei, F. Q., Hu, K. H., Xu, H., Zhao, L. Q., and Zhang, G. P.: A physics-based model to derive rainfall intensity-duration threshold for debris flow, Geomorphology, 351, 2020.

Zhou, W. and Tang, C.: Rainfall thresholds for debris flow initiation in the Wenchuan earthquake-stricken area, southwestern China, Landslides, 11, 877–887, 2014.